The interaction between the SEIS seismometer of the InSight Martian mission and a regolith simulant

Pierre Delage, Juan-Pablo Castillo Betancourt, Bernardo Caicedo Hormaza, Foivos Karakostas, Emmanuel de Laure, Philippe Lognonné, Daniele Antonangeli, Bruce Banerdt

The interaction between the SEIS seismometer of the InSight Martian mission and a regolith simulant

Pierre Delage[1], Juan-Pablo Castillo Betancourt[1,2], Bernardo Caicedo Hormaza[2], Foivos Karakostas[3], Emmanuel De Laure[1], Philippe Lognonné[4], Daniele Antonangeli[5], Bruce Banerdt[6]

[1] Ecole des Ponts ParisTech, Laboratoire Navier/CERMES, UMR CNRS 8205, France

[2] Universidad de Los Andes, Bogota, Colombia

[3] Istituto Nazionale di Geofisica e Vulcanologia, Bologna, Italia

[4] Université de Paris, Institut de Physique du Globe, UMR CNRS 7154, France

[5] Sorbonne Université, Institut de minéralogie, de physique des matériaux et de cosmochimie, UMR CNRS 7590, France

[6] Jet Propulsion Laboratory, NASA – CalTech, Pasadena CA, USA

Delage: ORCID 0000-0002-2101-5522 – Castillo Betancourt: ORCID 0000-0003-3123-4654 – Caicedo Hormaza: ORCID 0000-0003-4344-0914

Géotechnique, https://doi.org/10.1680/jgeot.21.00171

Institution of Civil Engineers, London, UK

KEYWORDS: laboratory tests; sands; soil–structure interaction

Abstract

A detailed investigation of the interaction between a Martian regolith simulant and the foot of a seismometer (SEIS) recently deployed on the surface of Mars within the NASA InSight mission has been conducted. A specific device used to investigate the SEIS/ground interaction was improved to provide accurate measurements of low forces and displacements, with a higher system stiffness and appropriate thermal insulation. A series of tests were carried out with a 60 mm diameter disk and the SEIS foot (disk with a spike in the disk centre). The maximum disk penetration in the loose sand used as simulant under the SEIS weight (10 N) was between 400 and 600 µm, with a tiny effect of the spike. Load cycles under various forces were performed to investigate the elastic interaction, with good reversibility and a linear change of the Young modulus with respect to the average vertical stress. The tests provided comparable values, showing that the Young modulus was around 20 MPa, compatible with that of loose terrestrial sands and agreeing well with the seismic wave velocities at surface (from laboratory experiments and from measuring on the surface of Mars the travel times of waves received by the SEIS seismometer).

Keywords: Laboratory tests, sands, soil structure interaction

1. Introduction

The Seismic Experiment for Interior Structure (SEIS, Lognonné et al. 2019, 2020) of the NASA (National Aeronautics and Space Administration) InSight mission on Mars (Interior Exploration using Seismic Investigations, Geodesy and Heat Transport, Banerdt et al. 2020) is the first seismometer ever deployed in direct contact with the surface of the planet Mars, in the footsteps of the Apollo Lunar Surface Experiments Package on the Moon (e.g. Latham et al. 1969, 1970; Bates et al. 1979) and 44 years after the landing of the two Viking seismometers in 1976 (these seismometers, placed on the landers with no direct contact with the ground, didn't provide any exploitable data). The InSight mission is a geophysical mission aimed at further understanding the structure of Mars and of the other terrestrial planets of the solar system. The main geophysical instruments deployed on Mars are a very high sensitivity seismometer (SEIS) funded by the French space agency (CNES - Centre National d'Etudes Spatiales) and the HP^3 instrument (Heat flow and Physical Properties Package), a self-penetrating dynamic probe (called the mole, 39.6 cm long and 2.7 cm diameter) funded by the German Institute for Planetary Research (DLR - Deutsches Zentrum für Luft- und Raumfahrt). The HP^3 instrument is designed to perform thermal conductivity measurements along the first 3 – 5 meters below the surface. The InSight lander that landed on Mars on 26 November 2018, is represented in the artist view of Figure 1, with both the SEIS (covered by a wind and thermal shield) and the HP^3 instruments deployed. Both are linked to the lander by tethers that transmit energy and data.

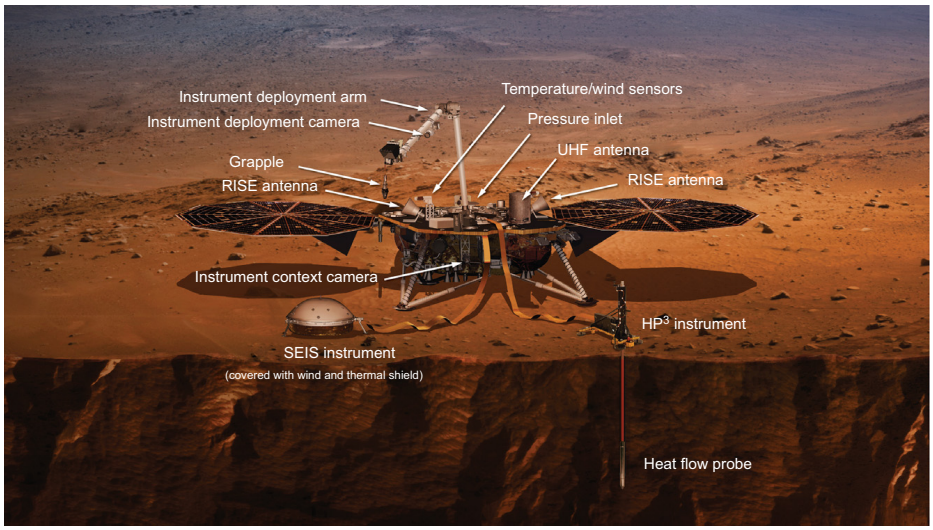

Figure 1. InSight NASA Lander concept and main instruments. Image credit JPL/NASA: https://mars.nasa.gov/insight/spacecraft/instruments/summary/

The Figure also shows the 2 m long Instrument Deployment Arm (IDA) and its grapple that deployed both SEIS and HP^3 on the ground. The IDA also carries a high-resolution Instrument Deployment (colour) Camera (IDC). The lander is also equipped with an Instrument Context Camera (ICC), a meteorological station including temperature, windspeed and pressure sensors, two RISE antennas (Rotation and Interior Structure Experiment) providing a precise location of the lander to accurately monitor the

movements of the planet from the Earth and an Ultra High Frequency antenna for data transmission. Energy is provided by two twin 1.8 m diameter solar panels with a power of 700 W each, on clear days.

The average size of the regolith particles on Mars was determined from thermal inertia measurements by the Viking lander and the Themis orbiter (Arvidson et al. 1989). The microscopic imagers of the Mars Exploration Rovers (MER - Spirit and Opportunity, 2004), Mars Science Laboratory (MSL - Curiosity, 2012) and Phoenix lander (2008) evidenced sorted dark grey basaltic sub-rounded to rounded fine sand particles (due to wind saltation under a 750 Pa atmospheric pressure), with diameter between 80 and 200 µm. This range is compatible with the average diameter (170 µm) derived from thermal inertia measured at the InSight landing site (160–230 J m^{-2} K^{-1} $s^{-1/2}$, Golombek et al., 2020). Bright red dust particles (2 – 5 µm) of slightly chemically altered basalt are also observed (Arvidson et al. 2004a et b, Golombek et al. 2006a and b and Goetz et al. 2010). Orbiter observations indicated that dust has been expelled by the rockets during landing at an average distance of 20 m around the InSight lander (Golombek et al. 2020).

Erreur ! Source du renvoi introuvable. shows a high-definition IDC photo of the Martian surface in the InSight landing site, showing the sand-like appearance of the regolith, with also some pebbles on the surface around.

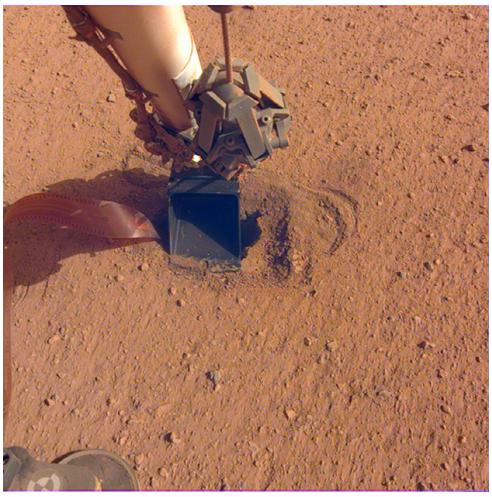

Figure 2. IDC photo showing the scoop of the Instrument Deployment Arm compressing the regolith above a hole developed around the self-penetrating mole during hammering. The scoop width is 7.6 cm (image credit JPL-NASA. IDC image acquired on Sol

A detailed geological description of the so-called “Homestead hollow” where the lander is located was presented by Golombek et al. (2020), from which the interpretative cross section of the landing site of Figure 3 has been extracted. It shows a typical regolith profile, with an around 3 m thick layer of relatively fine-grained impact generated regolith (3) that likely grades with depth into coarse, blocky ejecta (2) that overlies fractured basalt flows (1), with an estimated 10 m thick layer of blocky ejecta.

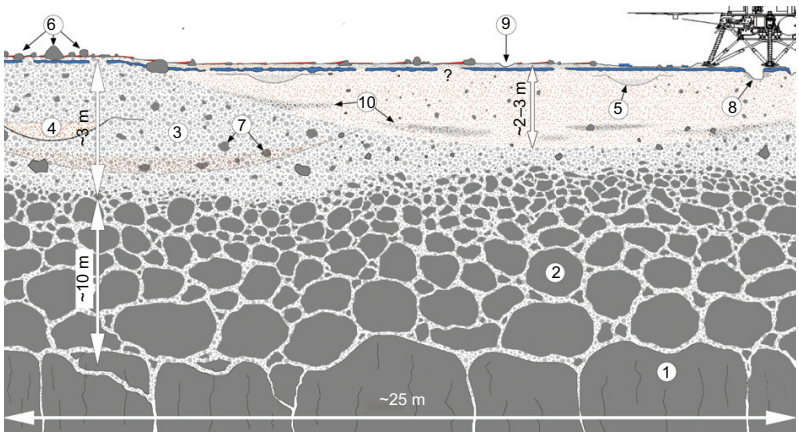

Figure 3. Interpretative cross-section of the shallow surface beneath the InSight lander (Golombek et al. 2020, Creative Commons CC BY license). 1: Fractured basalt flow; 2: Blocky ejecta; 3: Fine-grained impact generated regolith; 4, 5: Overlapping craters; 6: Rockier area; 7: Rocks embedded in regolith; 8: Pits opened by retro rockets during landing; 9: Surface divots; 10: Lens of ejecta from other craters.

This paper is devoted to further investigating the elastic interaction between the SEIS foot and a Martian regolith simulant, by using a specific device working at very low stresses and strains. In a first approach, the investigation was carried out under terrestrial gravity (9.81 m/s^2), higher than Mars' gravity (3.72 m/s^2). The aim of the program is to provide an estimation of the value of the axial elastic spring constant of the regolith simulant to allow for a theoretical modelling of the elastic interaction between the SEIS and the Martian regolith (see Fayon et al. 2018). From a seismology point of view, the elastic parameters of the surface regolith that can be derived from this experiment are also interesting to estimate the wave velocity in the near surface.

2. Material and methods

2.1.Introduction

The shape of the SEIS foot, designed based on a first series of tests carried out in a device developed at Ecole des Ponts ParisTech (Karakostas et al. 2013) is presented in **Erreur ! Source du renvoi introuvable.**. The foot consists of a disk with 60 mm diameter and a 20 mm long conic spike (10 mm diameter at its base) in its centre. As further detailed in Section 2.3, the device was improved to get a better accuracy in terms of displacement and force measurements.

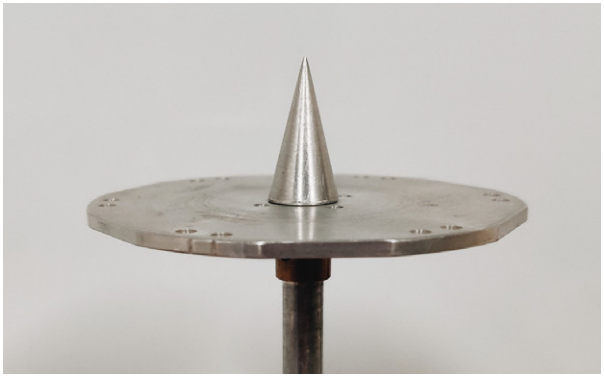

Figure 4. The shape of the SEIS foot. The conical spike has a maximum diameter of 10 mm.

2.2. Martian simulant

The selection of a relevant Martian regolith simulant is a difficult task (Seiferlin et al. 2008). Given the data provided by the MER, MSL and Phoenix missions and by thermal inertia measurement (see above), it was decided to adopt the Fontainebleau sand (NE34), a well sorted rounded sand with an average grain diameter D_{50} = 220 µm (a little bit larger than the 170 µm estimated value at the InSight site) and a uniformity coefficient C_u = 1,57 (the maximum and minimum void ratios are e_{min} = 0.54 and e_{max} = 0.86, respectively, Andria-Ntoanina 2011). The grain size distribution curve and a SEM photo showing the rounded shape of the grains are presented in Figure 5. As observed in **Erreur ! Source du renvoi introuvable.**, it is possible that the InSight regolith be less well sorted with more fine particles, but it is presently difficult to get further precision about the exact in-situ grain size distribution. Observations from previous missions also indicated a loose state of the regolith (Golombek et al. 2008) recently confirmed by local thermal measurements conducted at the surface by the HP^3 mole (Grott et al. 2021).

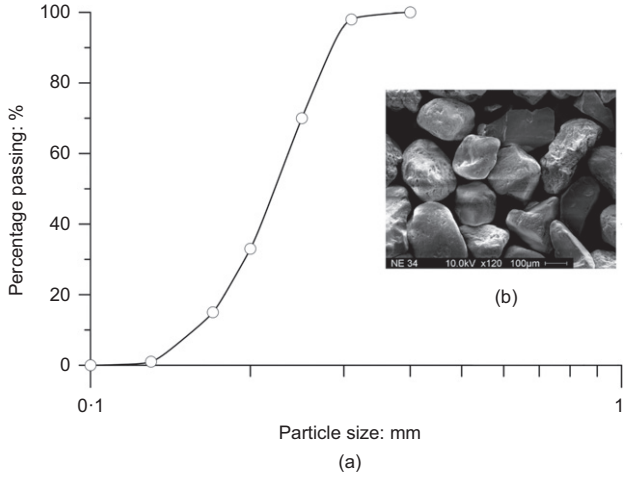

Figure 5. NE 34 Fontainebleau sand: a) Grain size distribution; b) Scanning electron microscope photo of the showing the subrounded grains (after Andria-Ntoanina 2011).

2.3. Experimental set-up

The precision of the experimental device used by Karakostas et al. (2013) was significantly improved by adopting high precision sensors for the measurements of both force and displacement (0.1µm), together with a stiff device designed to support the displacement ($6x10^{-4}$ N) transducer and a thermal insulation device of the whole system. The device (Figure 6) consists of a sand container of diameter 240 mm and height 120 mm placed on the plateau of a standard 100 kN triaxial press, allowing for upwards displacement at constant speed at 0.080 mm/min. The diameter of the container was constrained by the space available between the two rods of the triaxial press.

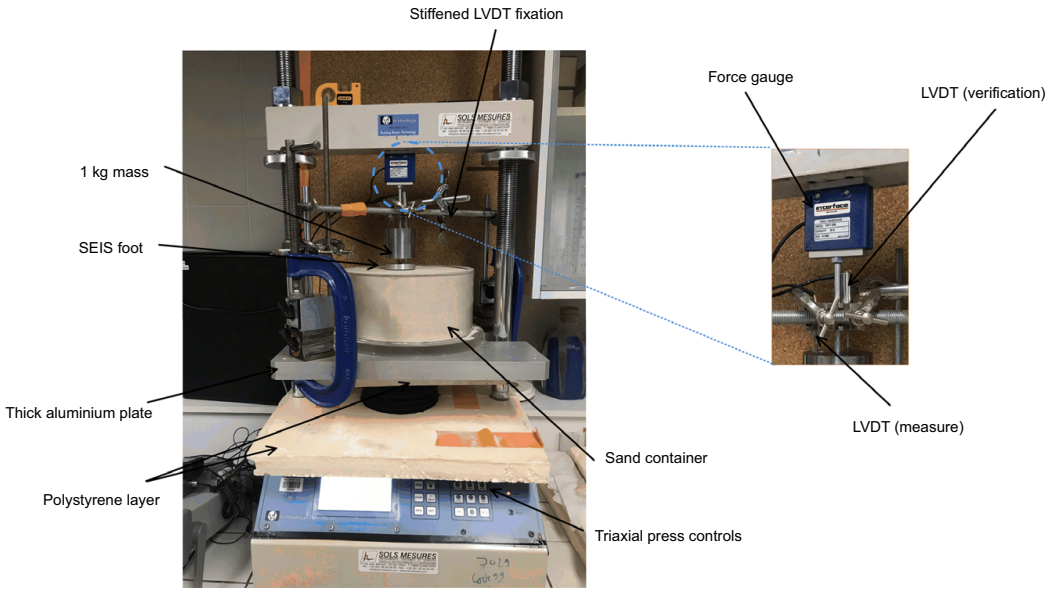

Figure 6. Experimental set-up, showing more details the fixation of the mass to the force gauge and the LVDTs providing the vertical displacement.

The relevance of the container dimensions with respect to boundary conditions was examined through elastic calculations based on Sneddon (1946)'s solution of a rigid circular plate on a semi-infinite elastic homogeneous space (see Appendix), with the following expression of the vertical displacement Δz:

$$\Delta z = \frac{\pi}{2}(1-\nu^2)\frac{\sigma_V R}{E} = \frac{F}{2RE}(1-\nu^2) \qquad (1)$$

where R is the disk radius, F the applied force, σ_v = F / π R^2 the average applied vertical stress, E the Young modulus and ν the Poisson coefficient. A Young modulus typical of loose sands (E = 20 MPa, Massarsch 2015) was adopted and ν was taken equal to 0.22 (Delage et al. 2017). Equation 1 allows analysing stresses on the boundaries of the mould, as shown in Figure 7. This analysis reveals slight changes in stress at the bottom (5% for σ_z and 2% for τ_{zx} of the vertical stress applied on the surface) and at the periphery, leading to a vertical strain ε_z = 0.001% at bottom (compared to 0.018% below the disk).

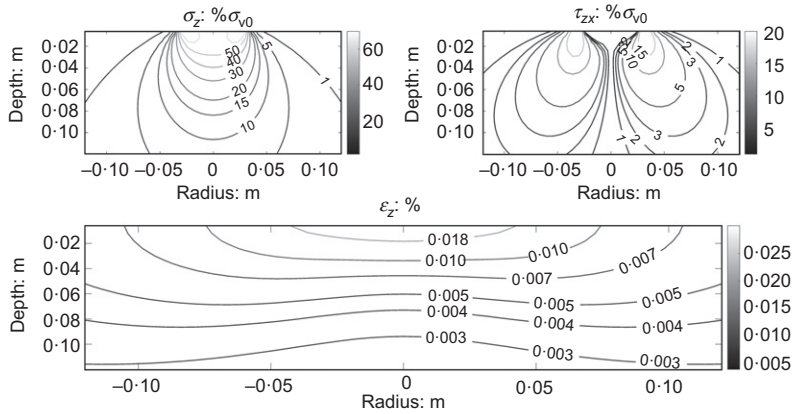

Figure 7. Elastic calculations of the vertical and shear stress (presented as percentages of the applied vertical stress) and of the vertical strain below the foot under the SEIS weight, based on Sneddon (1946)'s elastic solution.

Finite element elastic calculations were also carried out with the Plaxis code to account for possible effects due to the dimensions of the mould. Calculations made with the mould (240 mm diameter and 120 mm height) were compared to those with a much larger container comparable to a semi-infinite space (600 mm diameter and 550 mm depth). The differences obtained between the vertical displacements were 5.8 x 10^{-4} µm/N on the lateral boundary and 0.04 µm/N in the middle axis. They were considered small enough to conclude that the semi-infinite hypothesis used in Sneddon's approach was satisfactory for the mould used. Compared to the 220 µm average diameter of the sand grains, the small displacements calculated would result in a tiny movement of the grains at the interface with the container, with no significant effect on the disk penetration in the centre.

The option adopted in the work was to keep the real (Martian) foot dimensions by reusing the foot model used during the SEIS foot design (Karakostas et al. 2013), by putting it in contact with a simulant with grain size and shape comparable (albeit slightly larger) to those of the InSight regolith, and by loading it up to the force supported by each foot on Mars. The length scale used is 1 (e.g., $L^m/L^p=1$, where L^m is the length of the model and L^p is the prototype's length), leading to a disagreement in the similitude scale for stresses, that can be analysed by splitting stresses into those due to the seismometer weight σ_s (with a scale relationship of 1, e.g., $\sigma_s^m/\sigma_s^p = 1$) and those due to the self-weight of the soil σ_g, which is 2.64 times greater than on Mars. The match is not perfect along the earlier part of penetration, where the stresses due to soil self-weight predominates. However, once the load grows, the issue with similitude on stresses decreases because the induced stresses beneath the foot dominates over the self-weight stresses.

The SEIS foot is fixed at the bottom of a cylindrical mass of 1 kg, corresponding to the load supported by one SEIS foot under Mars' gravity, fixed to the horizontal rigid top beam of the press through a force gauge. The experiment is carried out by putting the spike of the foot in contact with the surface of the sand, prior to activating the upwards movement of the press. This allows for the progressive penetration, at a constant displacement rate, of the foot within the sand mass, until reaching the contact between the disk and the sample

surface. The spike penetration is monitored through the displacement rate of the press that has been carefully calibrated. Once the disk contacts the sand, a high accuracy in displacement monitoring is achieved by using a LVDT of 4.5 mm range with 0.1 µm resolution.

The force measurement was improved by using a 25 N range force gauge (Interface SMT1-25N). To reduce the noise in displacement measurements, a stiffer fixation system for the LVDT was adopted. As seen in Figure 6, the system is made up of two vertical rods strongly fixed on a thick aluminium plate placed on the plateau of the press along a diameter of the container, and of a horizontal rod strongly fixed to the two vertical ones. The 4.5 mm LVDT was fixed on this system, with its stem in contact with the upper side of the 1 kg mass. Another LVDT with a larger range of 20 mm, seen in Figure 6, has also been used for tilt verification. To the same aim, an insulation system from temperature changes and air movements has been set up, with particular attention paid to thermally insulate the two vertical rods of the triaxial press, because of the possible perturbations due to their thermal expansion/contraction on the displacement measurements. The insulation system consisted of a light prismatic box made up of 5 cm thickness expanded polystyrene and cork layer, placed around the device, as seen in Figure 8a, with a small access made through the box for the control system.

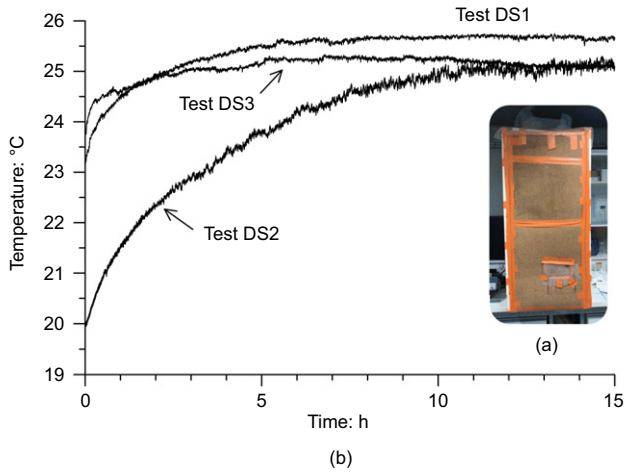

Figure 8. a) Thermal insulation of the device; b) temperature stabilisation is reached after 10 hours for tests DS1, DS2 and DS3 (see Table 1).

The performance of the insulating system was verified by performing several day/night temperature measurements carried out by means of a thermocouple (able to detect change in temperature smaller than 0.1°C, see **Erreur ! Source du renvoi introuvable.**) inside the box during up to three days. As shown in Figure 8b, thermal stabilization was attained one day after the box was placed around the device. Also, the sand container was insulated from possible thermal perturbations from the press by placing a thick polystyrene plate between the plateau and the thick plate. As observed in Figure 8b and **Erreur ! Source du renvoi introuvable.**, the resulting stabilization after 14 hours reduces temperature variations to the order of 0.1°C, which is found quite satisfactory.

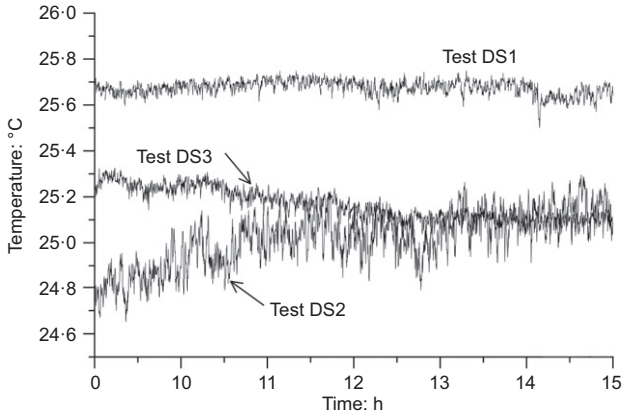

Figure 9. Temperature stabilization in tests DS1, DS2 and DS3 (see Table 1) made possible by the thermal insulation of the device, is of the order of 0.1°C.

2.4.Setting-up the low-density simulant specimen

Given that the low unit mass of the regolith (1400 kg/m^3 or even less, Golombek et al. 2008, Delage et al. 2017, Morgan et al. 2018, Grott et al. 2021), a dry funnel deposition procedure, already used by various authors (including Tatsuoka et al. 1979, Zlatovic and Ishihara 1997, Lade and Yamamuro 1997, Yamamuro and Wood 2004, Flitti et al. 2019) was adopted. To do so, the sand was gently poured at the centre of a container by using a funnel, keeping a zero falling height between the bottom end of the funnel and the top of the cone. The funnel was gently lifted by hand as the pile rises. An upper Plexiglas ring (8 cm in height) with the same diameter was placed on top of the container. Once the sand pile reached the right height, the ring was removed and the sand in excess was carefully erased to get a smooth horizontal upper plane surface. To minimise any disturbance, the sample was prepared close to the press and to a scale, on a mechanically insulating polystyrene layer. Once prepared, it was very carefully placed (no walking) on the scale for weighing, prior to be placed on the platen of the press. Once on the platen, the erased top surface of the sand was inspected to make sure that it stayed at the top of the container, which was the case. The unit mass of the deposited sand samples was found to be between 1.403 and 1436 kg/m^3 (see Table 1). It corresponds to an average density index I_d = 6 %, indicating a very loose state of the specimen.

2.5. Starting the test

Once the sample placed on the platen of the press, the thermal insulation box was placed and data acquisition started. As already mentioned, almost one day was necessary to reach temperature stabilization, a mandatory condition for proper displacement measurements. The plateau was moved at a low velocity of 0.08 mm/min to adequately monitor all relevant parameters. Various loading and unloading cycles were applied at different forces to investigate the dependence of the elastic response with respect to stress (see Table 1).

3. Experimental results

Most preliminary tests were aimed at establishing the validity of the device and at checking repeatability. To do so, it was found simpler to carried out tests with the 60 mm disk of diameter (without spike), because it allowed for an easier detection of the first sand/disk contact. As seen in Table 1, 10 tests were conducted with the disk. Once the performance of the system assessed, it was found that only 3 tests with the foot (disk + spike) were enough. The data obtained are presented in Table 1, including the values of the spring coefficient K_c determined from load cycles under various forces, and K_f from the final unloading and the Young moduli (E_c and E_f). The latter was derived under the hypothesis of elastic semi-infinite homogeneous half-space, as commented later on.

Table 1. Experimental program carried out.

N°	Unit mass kg/m^3	Max. p_t^* µm (± 0.1)	Max. force N (± 0.01)	Load cycles min – max N (± 0.01)	Slope K_c cycle MN/m (± 0.07)	Slope K_{fu} final unload MN/m (± 0.07)	Young modulus E_c cycle MPa (± 1.1)	Young modulus E_{fu} final unload MPa (± 1.1)
Disk only								
D1	1421	412.6	10.48	8.14 - 9.63	1.32	1.19	20.89	18.8
D2	1432	534.1	10.39	2.72 - 1.57 7.51 - 5.53	0.28 1.31	1.47	4.46 20.76	23.31
D3	1413	419.6	10.47	9.30 - 8.06	1.33	1.09	21.11	17.21
D4	1389	605.9	10.15	4.00 - 2.83	0.37	1.43	5.84	22.68
D5	1421	485.5	10.27	3.01 - 2.07 5.67 - 3.32	0.27 0.82	1.36	4.23 12.94	21.57
D6	1436	438.2	10.	9.46 - 7.87	1.23	1.47	19.53	23.31
D7	1423	392.5	10.01	6.92 - 5.62	1.03	0.93	16.38	14.71
D8	1409	605.4	10.97	3.12 - 1.77 5.53 - 3.02	0.63 1.15	0.76	10.03 18.17	11.97
D9	1428	348.6	9.80	8.77 - 7.44	1.16	1.53	18.37	24.27
D10	1435	408.3	10.31	8.98 - 6.37	1.47	1.37	23.25	21.73
Disk + spike								
DS1	1428	607.4	10.6	8.55 6.49	1.11	1.087	17.59	17.24
DS2	1403	598.4	9.91	8.81 - 6.77	1.26	0.825	20.02	13.09
DS3	1418	611.3	10.56	- 7.40	1.18	0.936	18.65	14.85

* *p_t: penetration*

3.1. Penetration tests with the disc

10 tests were carried out with the disk up to a maximum force of 10 N, i.e., the force applied on the ground by each SEIS foot on Mars. Half of them were performed to determine, through a load cycle, the elastic response under 10 N. 5 others were performed under smaller stresses to characterize the variation of the elastic response with stress. All final unloading sequences were also used to determine the K_f coefficients and the E_f Young moduli, as indicated in Table 1.

Erreur ! Source du renvoi introuvable. shows the penetration curves of the 10 tests in terms of force (N) with respect to the penetration distance (µm) monitored by the 4.5 mm range LVDT. The Figure shows some variability in the maximum penetration observed that ranges between around 400 µm for 7 tests and around 600 µm for the other 3. The responses at the beginning of the series of the 7 tests show a stronger increase in force with respect to the displacement. A comparable slope is however reached for the three other tests after a penetration of 300 µm.

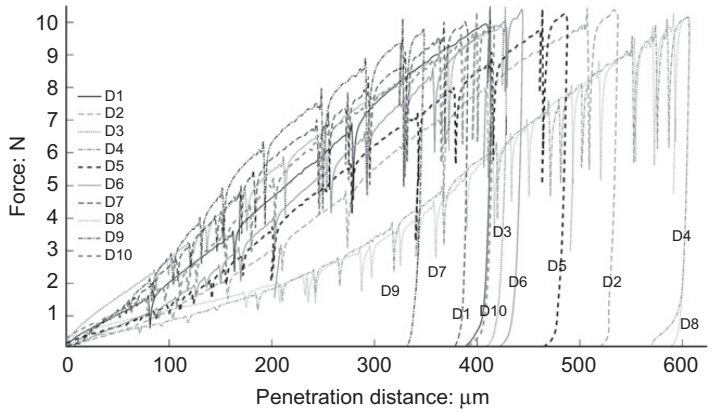

Figure 10. Force-penetration curves for the 10 tests performed with the disc.

All curves show many spikes corresponding to sudden decreases in force, followed by a force recovery along several micrometres that brings back the curve along the initial one that are typical of slip and stick phenomena (Cain et al. 2001).

As indicated in Table 1, the elastic response under the SEIS weight (10 N) and thus very small stresses was investigated through cycles in force. Figure 11 shows a cycle performed during test D10 between 8.98 and 6.37 N (force amplitude of 2.61 N), with a resulting penetration response between 395.65 and 397.4 µm (amplitude of 1.75 µm). The curve shows that the decrease in force, resulting from stopping and reversing the direction of the movement of the plateau, is not instantaneous, with a progressive decrease in force between 9.67 and 9.29 N occurring along 0.8 µm, followed by a frank linear decrease in both force and displacement. A very slight hysteresis is observed, with a difference of 0.2 µm between the two points at 8 N, showing quite a good reversibility and linearity of the response. A value of an elastic spring constant $\Delta F/\Delta d$ of 1.47 x 10^6 N/m is derived from the graph.

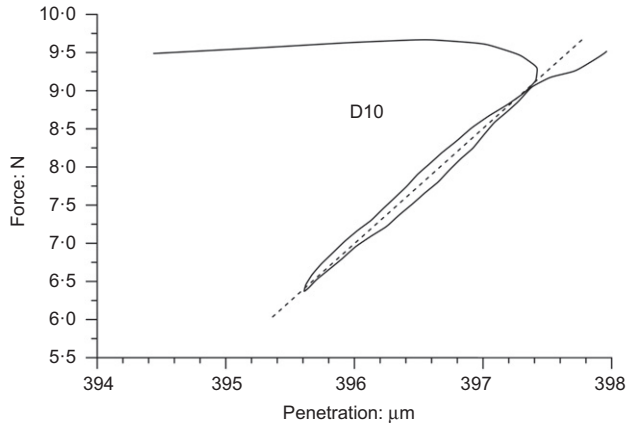

Figure 11. Load-unload cycle performed between 8.98 and 6.37 N in test 10 (disk only). The stiffness coefficient given by the slope is k = 1.47 x 10^6 N/m.

3.2.Penetration tests with the foot (disk + spike)

The difficulty was to accurately determine the first contact between the spike and the sand, an impossible task if based on force measurement. Since it was easier to detect the contact between the disk and the sand, it was decided to set this point at zero and to plot back the penetration of the spike, as shown in Figure 12a. The curve shows that the penetration of the spike along the first 17 mm (17 000 µm to compare to the 400 – 600 µm of disk penetration) provides no significant added effect of the spike in the loose sand (added contribution between 0.14 and 0.54 N). The Force/Penetration curve of test DS1 is presented in Figure 12 a and b, showing no significant force mobilisation below 3 mm and a maximum force of 0.14 N obtained just before the sand/disk contact is reached. The monitored forces also give an idea of the force gauge accuracy that can be estimated $\pm$ 0.01 N. The sudden drops in force previously observed with the disk and typical of stick and slip are also seen with the cone (at 5 200 and 9 100 µm).

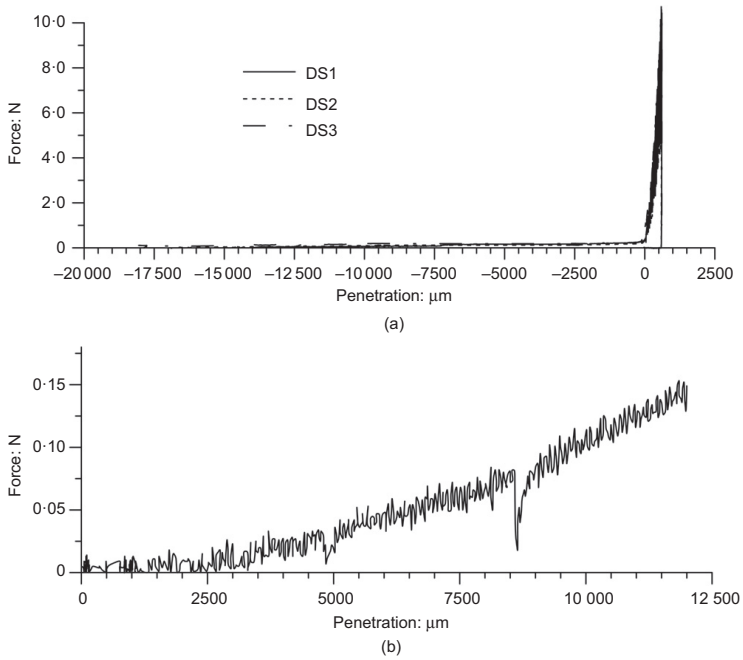

Figure 12. a) Force-penetration curves for the 3 tests performed with the foot (disk+spike). Note that the force significantly increases once the disk contacts the sand surface. The start of the disk/sand contact is taken as 0 for the x-axis, and the curves are started at a point obtained by subtracting the length of the spike (- 20 000 µm), b) Detailed force penetration curve of the spike alone for test DS1, with a maximum force of 0.14 N reached just before sand/disk contact. Two stick-slips are observed at around 4800 and 8600 µm.

The curves illustrating the interaction between the foot and the sand (Figure 13) are similar to those obtained without the spike, confirming the tiny effect of the spike. A maximum penetration of 600 µm was obtained in these tests, like in three of the tests with the disk only (**Erreur ! Source du renvoi introuvable.**). Reversible load cycles similar to that presented in Figure 11 were also observed, confirming little effect of the spike on the elastic response.

4. Interpretations and discussion

4.1.General considerations

The challenge of setting up an experimental device able to deal with very low stress and strain has been met, thanks to special care devoted to the thermal insulation and to the stiffness of the device, resulting in a precision of around 0.1 µm in displacements. The maximum disk penetration obtained with our device under the weight of the SEIS (under Mars gravity - around 10 N) is between 400 and 600 µm, whereas the average grain diameter of the Fontainebleau sand, 220 µm, is around two to three times smaller. The low stress in the area affected by the disk penetration hence results in quite small plastic strains that correspond to the displacement of a limited number of grains below the sample surface, illustrated by the slope of the curves of **Erreur ! Source du renvoi introuvable.**. The data of **Erreur ! Source du renvoi introuvable.** and Figure 13 show that the force reached

at a displacement corresponding to the average grain diameter is between 2 and 7.5 N. This shows that the beginning of the curve is influenced by the roughness of the surface, that is controlled by the arrangement of the grains. Besides possible effects of local changes in density, this may be the explanation for the less pronounced start of the curves reaching 600 µm. Conversely, the reversible load cycles illustrate a small elastic response of 1.3 – 2 µm in vertical displacement, to be compared to the 220 µm average diameter of the grains, indicating a limited reorganisation of the grain assembly. The elastic response should mainly be governed by the reversible stress release/recompression at grain contacts, following the Hertz-Mindlin contact theory (Hertz 1882, Mindlin 1949).

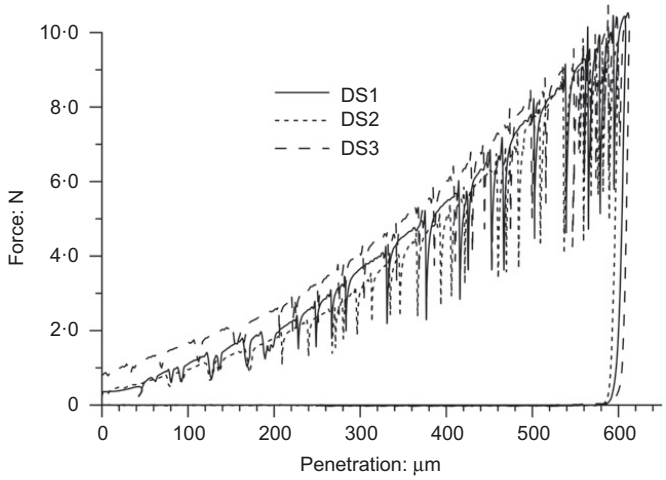

Figure 13. Force penetration curves for the 3 tests carried out with the foot (disk + spike) once the spike has fully penetrated the sand and the disk is in contact with the sand.

When comparing the penetration curves and the close values of the elastic spring constants of the foot and the disk only (Table 1), no significant added effect of the spike was observed, showing that there is space enough in the loose contracting sand to accommodate the thin spike without any added strength. This probably also holds for the InSight regolith, the low density of which has been confirmed by both the development of a pit around the mole at the start of the penetration of the HP^3 instrument (Golombek et al. 2020) and by some in-situ thermal conductivity measurements that provided estimated unit mass values around 1200 kg/m^3 (Grott et al. 2021). Some pebbles, like those observed in **Erreur ! Source du renvoi introuvable.**, have also been observed in the excavations created by the rockets during landing and in the mole pit. The possibility of not having full penetration of one of the SEIS feet due blocking by a pebble cannot be completely eliminated. However, the thin shape of the spike is optimum in this regard, allowing easier deviation of the spike along a small enough pebble, and full penetration in the loose regolith.

4.2.Elastic interpretation of the response

Based on the measurements of elastic spring constants K_v presented in Table 1 and on the simplifying assumption of homogeneous linear and isotropic behaviour of the sand, one

derived the Young moduli for all the cycles performed (see Table 1) based on the following expression derived from Sneddon's Equation (1):

$$E = \frac{k_v(1-\nu^2)}{2R} \quad (2)$$

The elastic strain increment corresponding to the force cycle of Figure 11 is equal to 6 x 10^{-5}, showing that the Young moduli are determined at small deformations, not far from the range of those derived from bender element measurements (10^{-5} - 10^{-6}), as done in Delage et al. (2007). The changes in Young modulus with respect to the average vertical stress at surface are presented in Figure 14 (given the negligible effect of the spike, the calculations for the foot have also been made by using Sneddon's solution).

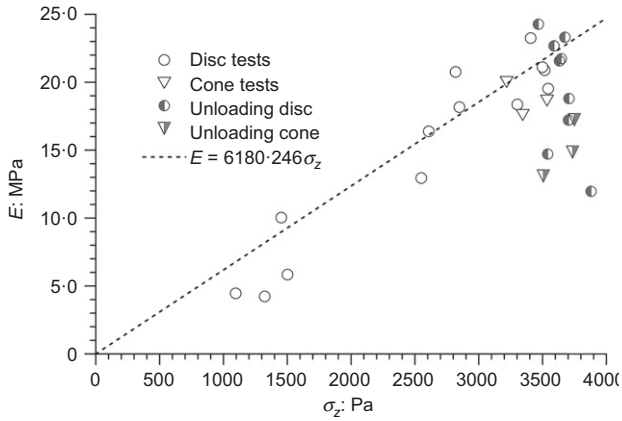

Figure 14. Changes in Young modulus with respect to the average vertical stress at surface. Data are derived from load cycles tests and from the final unloading step.

In the area corresponding to the SEIS weight (around 3.5 kPa), some dispersion is observed, with *E* values derived from load cycles between 17.59 and 23.25 MPa. This is an indication of possible changes in local density of the sample at the contact area with the disk/spike, probably enhanced by the small number of grains mobilised by the low applied stress, or for other reasons that are not yet clear, including possible hysteretic material behaviour of the sand. Averaging the values between 3 and 3.5 kPa yields an average *E* value of 20.07 MPa (note that, for some reasons, some of the monotonic unloading coefficients at maximum force stay well below the line, with values as small as 11.97 – 14.85 MPa). Possible effects of changes in Young modulus with depth, suggested by the data of Figure 14, were investigated by carrying out finite elements calculations with a linear change of E with depth, in a model composed of 12 layers of 1 cm thickness. The difference in settlement at surface was found equal to 0.0468 µm/m, indicating negligible effects of changes in Young modulus with depth.

The linear changes in Young modulus with respect to changes in average vertical stress (a value easy to calculate under a rigid plate) observed in Figure 14 are distinct from the well-known power law that relates the Young modulus with the confining stress, defined by the two following equations (e.g. Santamarina et al. 2001):

$$V_p = \alpha \left(\frac{p}{1\ kPa} \right)^{\beta} \quad (3)$$

and

$$E = \rho V_p{}^2 \left(\frac{3 - \frac{4}{l^2}}{l^2 - 1} \right) \quad (4)$$

with $l = \sqrt{\frac{2(1-\nu)}{1-2\nu}}$

where p is the mean stress, and α (m/s) and β (-) two fitted parameters. Delage et al. (2017) obtained β = 0.3 and ν = 0.22 on three different (more angular) Martian simulants. Following Santamarina et al. (2011), it was found more relevant to adopt, for subrounded grains, a slightly smaller value of 0.28, which results in having a power law with β = 0.56, slightly larger than the 0.5 value commonly adopted for sands (e.g., Hardin and Black 1966, Oztoprak and Bolton 2013). The significant difference with the linear changes observed in Figure 14 is related to the use of average vertical stress σ_z instead of mean stress ((σ_z + 2 σ_x /3, since σ_x = σ_y). Inspection of the Sneddon's expressions of σ_z, σ_x and σ_y (see Appendix) shows that the relation between σ_z and p is far from being simple, with the added difficulty of properly estimating the relevant layer thickness needed to estimate p under the disk.

Knowing E allows for the calculation of the other parameters governing the SEIS/ground interaction used in Fayon et al. (2019) in their modelling of the SEIS ground interaction, i.e., the horizontal spring coefficient k_h and the torque C_h (Poulos and Davis 1974):

$$k_h = \frac{16\ \mathrm{ER}(1-\nu)}{(7-8\nu)(1+\nu)} = 1.17 \times 10^6 N/M \quad (5)$$

$$C_h = \frac{4\ \mathrm{ER}^3}{3(1-\nu^2)} = 756.6\ N.m \quad (6)$$

Given that the Young modulus has been derived at a strain of 6 x 10^{-5}, another interesting seismic parameter that can be derived is the compression wave velocity at surface, according to the following equation:

$$V_p = \sqrt{\frac{\mathrm{E}(1-\nu)}{\rho(1+\nu)(1-2\nu)}} \quad (7)$$

in which ρ is the regolith unit mass. Adopting E = 20 MPa, ρ = 1.400 kg/m^3 and ν = 0.22 yields a value of compression wave velocity of 128 m/s, in the expected range for sands under low confinement. Interestingly, this is also in a good agreement with the in-situ velocities at the surface of Mars derived from analysing the seismic signals received by SEIS from HP^3 hammering at around 0.3 m deep, and 1.1 m away, equal to 118 $\pm$ 34 m/s for a surface layer approximately 30 cm thick (Lognonné et al. 2020).

However, note that these satisfactory agreements do not necessarily prove that our experiment exactly reproduces the situation on Mars. Some limitations have been discussed above in this regard, both in terms of simulant and scale effects. The calculations here are also made based on a simplifying assumption of an equivalent homogeneous isotropic semi-

infinite medium, whereas it is known that there is an increase of the elastic modulus of granular media with increased mean stress, as shown in Figure 14. Beside the detailed geological examination of the surface (Golombek et al. 2020), further investigations are presently carried out in this regard within the Near Surface Working Group of the InSight Science Team, based on visual and geological analyses, on the local measurements of thermal inertia, on the seismic signals received by SEIS and on the thermal data provided by HP^3. Based on thermal inertia measurement, a possibility could be to have a finer material with some cohesion, which would also be compatible with the very low density suspected.

5. Conclusions

Some improvements were made on the specific device that allowed to design the final shape of the SEIS foot (Lognonné et al. 2019) and to provide the first estimation of the elastic parameters governing the interaction between a Martian simulant and the SEIS foot as analysed in Fayon et al. (2018). To successfully carry out accurate tests in conditions of very low stresses (< 4 kPa) and displacements (< 600 µm), particular care was taken in optimising measurements by using a stiff system to support the container and the LVDT gauges, by using an adapted force gauge and a complete thermal insulation device, allowing to get rid of any perturbation that could result from the thermal expansion/contraction of the loading system, provided a time period of 24h was waited for to ensure a constant temperature with variations smaller than 0.5°C. This high precision device allowed to successfully carry out interaction tests between both a disk and the foot. The tests showed that, under the SEIS weight, the maximum penetration in the simulant adopted was around 600 µm, i.e., less that the thickness of a layer made up of 3 grains of Fontainebleau sand, a well graded rounded sand with an average grain diameter of 220 µm. As a consequence, the start of the penetration curves was affected by the roughness of the specimen surface, who resulted in having maximum penetration between 400 and 600 µm, i.e., around twice the diameter of a grain. The large number of tests conducted on loose specimens with dry unit mass around 1400 kg/m^3 (density index of 6%) showed reasonable repeatability, with however some dispersion in measured modulus related to possible changes in local density. The elastic response was investigated by conducting stress cycles at various force levels that provided fairly reversible responses with small hysteresis. A simplified analysis considering a homogeneous elastic isotropic semi-infinite medium was carried out to determine the dependency of the Young modulus with respect to the average vertical stress. The linearity observed was distinct to the power law observed with respect to the mean stress, a value difficult to estimate in our case. It was also shown that the effect of the spike in a loose regolith was not significant. The order of magnitude of the Young modulus under the SEIS foot is 20 MPa, a reasonable value for loose sand on the Earth. This value was found compatible with previous laboratory estimations of the surface compression wave velocity and also with in-situ seismic measurements carried out on the InSight landing site by SEIS, from the hammering sessions of HP^3. The data obtained from this improved system will allow for a better determination of the SEIS – regolith interaction and of the resulting resonance frequencies (Fayon et al. 2018). They of course could be improved in the future, once better knowledge about the regolith simulant is obtained. They can also be used for

the resonance frequencies of the lander itself, that appeared to also have significant effects on the SEIS measurements.

6. Acknowledgements

The work presented in this paper is part of the second author's PhD thesis, funded by a joint support from both Ecole des Ponts ParisTech (France) and Universidad de los Andes (Bogota, Colombia). The work was also supported by CNES (Centre National d'Etudes Spatiales), the French Spatial Agency and Institut de Physique du Globe (Université Paris - Cité). The authors want to acknowledge the help provided by the CERMES technical team, with the contributions of Loic Lesueur for the setting up of the experiment and of Xavier Boulay for the sensor installation, calibration and data acquisition. The suggestions made by Baptiste Chabot and by Julieth Monroy (from Universidad de los Andes, Bogota) for improving the experimental setup and analysis were also key to succeed in this work. This paper is InSight contribution 209.

7. References

Andria-Ntoanina, I. (2011). Caractérisation dynamique de sables de référence en laboratoire - Application à la réponse sismique de massifs sableux en centrifugeuse. Thèse Université Paris-Est - Ecole des ponts ParisTech.

Arvidson R.E., Guinness E. A., Dale-Bannister M., Adams J., Smith M., Christensen P.R., Singer N.B. (1989). Nature and Distribution of Surficial Deposits in Chryse Planitia and Vicinity, Mars. Journal of Geophysical Research 94 (b2), 1573-1587.

Arvidson, R. E. et al. (2004a). Localization and physical properties experiments conducted by Spirit at Gusev crater. Science 305, 821–824.

Arvidson, R. E. et al. (2004b). Localization and physical properties experiments conducted by Opportunity at Meridiani Planum. Science 306, 1730–1733.

Banerdt W.B., Smrekar S.E., Banfield D., Giardini D., Golombek M., Johnson C.L., Lognonné P., Spiga A, Spohn T. et al. (2020). Initial results from the InSight mission on Mars. Nature Geoscience (13), 183–189.

Bates J.R., W.W. Lauderdale, H. Kernaghan (1979). ALSEP Termination Report, NASA Reference Publication Series, NASA-RP-1036, S-480, 914-40-73-01-72, p. 162

Cain, R., Page, N., and Biggs, S. (2001). "Microscopic and macroscopic aspects of stick- slip motion in granular shear". *Physical Review E*, Vol 64, No 016413. pp 1-8.

Delage, P., Karakostas, F., Dhemaied, A., Belmokhtar, M., Lognonné, P., Golombek, M., De Laure, E., Hurst, K., Dupla, J. C., Kedar, S., Cui, Y. J., & Banerdt, B. (2017). An Investigation of the Mechanical Properties of Some Martian Regolith Simulants with Respect to the Surface Properties at the InSight Mission Landing Site. Space Science Reviews, 211(1–4), 191–213. https://doi.org/10.1007/s11214-017-0339-7

Fayon, L., Knapmeyer-Endrun, B., Lognonné, P., Bierwirth, M., Kramer, A., Delage, P., Karakostas, F., et al. (2018). A Numerical Model of the SEIS Leveling System Transfer Matrix and Resonances: Application to SEIS Rotational Seismology and Dynamic Ground Interaction. In Space Science Reviews (Vol. 214, Issue 8). Springer Nature B.V. https://doi.org/10.1007/s11214-018-0555-9

Flitti, A., Della, N., De Kock, T., Cnudde, V., & Verástegui-Flores, R. D. (2019). Effect of initial fabric on the undrained response of clean Chlef sand. *European Journal of Environmental and Civil Engineering*, 1-16.

Goetz, W., Pike, W. T., Hviid, S. F., Madsen, M. B., Morris, R. V., Hecht, M. H., Staufer, U.et al. (2010). Microscopy analysis of soils at the Phoenix landing site, Mars: Classification of soil particles and description of their optical and magnetic properties. Journal of Geophysical Research E: Planets, 115(8), 1–23. https://doi.org/10.1029/2009JE003437.

Golombek, M.P., J. A. Grant, L. S. Crumpler, R. Greeley, R. E. Arvidson, J. F. Bell III, C. M. Weitz, R. Sullivan, P. R. Christensen, L. A. Soderblom, and S. W. Squyres (2006a). Erosion rates at the Mars Exploration Rover landing sites and long-term climate change on Mars. J. Geophys. Res., 111, E12S10, doi:10.1029/2006JE002754.

Golombek, M. P. , L. S. Crumpler, J. A. Grant, R. Greeley, N. A. Cabrol, T. J. Parker, J. W. Rice Jr., J. G. Ward, R. E. Arvidson, J. E. Moersch, et al. (2006b). Geology of the Gusev cratered plains from the Spirit rover transverse. Journal of Geophysical Research, Vol. 111, E02s07, doi:10.1029/2005je002503.

Golombek M.P., A.F.C. Haldemann, R.A. Simpson, R.L. Fergason, N.E. Putzig, R.E. Arvidson, J.F. Bell III., M.T. Mellon (2008). Martian surface properties from joint analysis of orbital, Earth-based, and surface observations, in The Martian Surface: Composition, Mineralogy and Physical Properties, ed. by J.F. Bell III. (Cambridge University Press, Cambridge, 2008), pp. 468–497. Chap. 21

Golombek, M., Warner, N. H., Grant, J. A., Hauber, E., Ansan, V., Weitz, C. M., Williams, N., Charalambous, C., Wilson, et al. (2020). Geology of the InSight landing site on Mars. Nature Communications, 11(1), 1–11. https://doi.org/10.1038/s41467-020-14679-1

Grott M., T. Spohn, J. Knollenberg, C. Krause, T.L. Hudson, S. Piqueux et al. (2021). Thermal Conductivity of the Martian Soil at the InSight Landing site from HP3 Active Heating Experiments. Journal of Geophysical Research - Planets, doi 10.1002/essoar.10506340.1.

Hardin, B. O. & Black, W. L. (1966). Sand stiffness under various triaxial stresses. J. Soil Mech. Found. Div. ASCE 92, No. SM2, 667 – 692.

Hertz, H. (1882), ‘‘Ueber die Berührung fester elastischer Körper’’ (‘‘On the fixed elastic body contact’’), Journal für die reine und angewandte Mathematik (Crelle), Vol. 92, pp. 156-71.

Karakostas F., P. Delage, E. De Laure, A. Dhemaied, J.C. Dupla, A.M. Tang, Y.J. Cui. 2013. The geotechnical properties of some Mars regoliths simulants and their interaction with the SEIS foot. Research report submitted to IPGP.

Latham G.V., M. Ewing, F. Press, G. Sutton, J. Dorman, N. Toksoz, R. Wiggins, Y. Nakamura, J. Derr, F. Duennebier, Passive seismic experiment, in *Apollo 11 Preliminary Science Report*, NASA, vol. SP-214 (1969), pp. 143–161

Latham, G.V., M. Ewing, F. Press, G. Sutton, J. Dorman, Y. Nakamura, N. Toksöz, R. Wiggins, J. Derr, F. Duennebier, Passive seismic experiment. Science **167**, 455–457 (1970). https://doi.org/10.1126/science. 167.3918.455

Lognonné, P., Banerdt, W. B., Giardini, D., Pike, W. T., Christensen, U., Laudet, P., de Raucourt, S., Zweifel, P., Calcutt, S., Bierwirth, M., Hurst, K. J., Ijpelaan, F., et al. (2019). SEIS: Insight’s Seismic Experiment for Internal Structure of Mars. Space Science Reviews (Vol. 215, Issue 1). https://doi.org/10.1007/s11214-018-0574-6

Lognonné P., Banerdt W. B., Pike W. T., Giardini D., Christensen U., Garcia R. F., Kawamura T., Kedar S., Knapmeyer-Endrun B., Margerin L., Nimmo 10, Panning M., Tauzin B. et al. (2020). Constraints on the shallow elastic and anelastic structure of Mars from InSight seismic data. Nature Geoscience, https://doi.org/10.1038/s41561-020-0536-y

Massarsch, K.R. 2015. Determination of shear modulus of soil from static and seismic penetration testing. Jubilee Volume. Proceedings in honour of Prof. A. Anagnostopoulos, Technical University of Athens. Ed. M. Kavvadas. Athens 2015. Tsotras ISBN: 978-618-5066-30-7, pp. 335 – 352.

Mindlin, R. (1949), ‘‘Compliance of elastic bodies in contact’’, Transactions of the ASME, Journal of Applied Mechanics, Vol. 16 No. 3, pp. 259-68.

Morgan P., M. Grott, B. Knapmeyer-Endrun, M. Golombek, P. Delage, P. Lognonné, S. Piqueux et al. 2018. “A Pre-Landing Assessment of Regolith Properties at the InSight Landing Site.” Space Science Reviews. https://doi.org/10.1007/s11214-018-0537-y.

Oztoprak S. and Bolton M.D. (2013). Stiffness of sands through a laboratory test database. Géotechnique 63(1), 54 - 70.

Poulos H. G. & Davis E.H. (1974). Elastic Solutions for Soil. Series in Soil Engineering, Wiley.

Sneddon, I. N. (1946). Boussinesq's problem for a flat-ended cylinder. Mathematical Proceedings of the Cambridge Philosophical Society, 42 (1) 29 – 39, doi 10.1017/S0305004100022702

Santamarina J.C., Klein K.A., Fam M.A. 2001. *Soils and Waves* (Wiley, New York)

Tatsuoka, F., Iwasaki, T., Yoshida, S., Fukushima, S., & Sudo, H. (1979). Shear modulus and damping by drained tests on clean sand specimens reconstituted by various methods. Soils and Foundations, 19(1), 39–54. doi:10.3208/ sandf1972.19.39

Lade PV, Yamamuro JA. (1997). Effects of non-plastic fines on static liquefaction of sands. Canadian Geotechnical Journal; 34(6): 918–28

Vaid, Y. P., Sivathayalan, S., & Stedman, D. (1999). Influence of specimen-reconstituting method on the undrained response of sand. Geotechnical Testing Journal, 22(3), 187–195. doi:10.1520/GTJ11110J

Wood, F. M., Yamamuro, J. A., & Lade, P. V. (2008). Effect of depositional method on the undrained response of silty sand. Canadian Geotechnical Journal, 45(11), 1525-1537.

Yamamuro, J. A., & Wood, F. M, . (2004). Effect of depositional method on the undrained behavior and microstructure of sand with silt. Soil Dynamics and Earthquake Engineering, 24(9-10), 751-760.

Zlatovic, S., & Ishihara, K. (1997). Normalized behavior of very loose non-plastic soils: Effects of fabric. Soils and Foundations, 37(4), 47–56. doi:10.3208/sandf.37.4_47

8. Appendix

The normal and stress fields presented in Figure 7 are based on Sneddon’s solution for a cylindrical shaped indenter. The expressions are presented in more detail below.

Sneddon (1946) provided, from an elastic analysis based on Boussinesq’s solution, the following expressions for the stress and strain field under a rigid loaded plate:

$$\sigma_z = \frac{3F}{2\pi} \cdot \frac{z^3}{R^5} \tag{8}$$

$$\sigma_x = \frac{3F}{2\pi} \cdot \frac{x^2 z}{R^5} - \frac{m-2}{3m}\left[-\frac{1}{R\cdot(R+z)} + \frac{(2R+z)x^2}{(R+z)^2 R^3} + \frac{z}{R^3}\right] \tag{9}$$

$$\sigma_y = \frac{3F}{2\pi} \cdot \frac{y^2 z}{R^5} - \frac{m-2}{3m}\left[-\frac{1}{R\cdot(R+z)} + \frac{(2R+z)y^2}{(R+z)^2 R^3} + \frac{z}{R^3}\right] \tag{10}$$

$$\tau_{xy} = \frac{3F}{2\pi} \cdot \frac{xyz}{R^5} - \frac{m-2}{3m}\left[\frac{(2R+z)xy}{(R+z)^2 \cdot R^3}\right] \tag{11}$$

$$\tau_{xz} = \frac{3F}{2\pi} \cdot \frac{xz^2}{R^5} \tag{12}$$

$$\epsilon_z = \sigma_z / E \tag{13}$$

$$p_t = \frac{1+\nu}{2\pi E} \cdot \left[\frac{z^2}{R^3} - \frac{(1-2\nu)x}{R}\right] \cdot F \tag{14}$$

in which *F* is the force applied on the disk, *z* the depth, x and y the horizontal distance from the axis, $R = \sqrt{x^2 + y^2 + z^2}$, p_t the penetration and $m = 1/\nu$.